J. Fluid Mech. (2011), *vol.* 685, *pp.* 1–22.
doi:10.1017/jfm.2011.263

Oscillatory motion of a viscoelastic fluid within a spherical cavity

Julia Meskauskas[1], **Rodolfo Repetto**[2]† **and Jennifer H. Siggers**[3]

[1] Department of Engineering of Structures, Water and Soil, University of L'Aquila, Strada provinciale per Monticchio, Monticchio, 67100 L'Aquila, Italy

[2] Department of Civil, Environmental and Architectural Engineering, University of Genoa, Via Montallegro 1, 16145 Genova, Italy

[3] Department of Bioengineering, Imperial College London, London SW7 2AZ, UK

(Received 7 February 2011; revised 23 May 2011; accepted 7 June 2011; first published online 21 September 2011)

We study the motion of a viscoelastic fluid within a rigid spherical cavity with the aim of improving understanding of the motion of the vitreous humour in the human eye. The flow of vitreous humour leads to traction on the retina, which, once the retina is torn or damaged, can cause it to detach from the choroid, leading to loss of sight if left untreated. In the first part of the paper we investigate the relaxation behaviour of the fluid, the transient flow that would be observed in the stationary sphere starting from non-stationary initial conditions. For a general viscoelastic fluid we calculate the growth rates and eigenfunctions associated with the system, and we discuss two particular rheological models of the vitreous humour taken from the literature. In the second part of the paper we consider forced oscillations of the fluid, due to small-amplitude rotations of the sphere about a diameter, representing saccades of the eyeball. We conclude with a discussion of the possible occurrence of resonant phenomena and their clinical relevance.

Key words: biomedical flows, viscoelasticity

1. Introduction

The vitreous chamber of the eye has a near-spherical shape and is filled with vitreous humour. This is a transparent fluid with complex mechanical properties due to the presence of a network of collagen fibrils and polyanionic hyaluronan macromolecules of high molecular weight (Bishop 2000). Measurement of the rheological properties of the vitreous humour is extremely challenging, owing to its lubricating ability and its fragile and inhomogeneous network structure. In addition, the location within the vitreous chamber from which the sample is taken, details of the experimental apparatus, and the duration from the dissection to the experiment are all expected to influence the measured values.

Lee, Litt & Buchsbaum (1992) performed a systematic study of the rheological properties of the human vitreous humour. The shear behaviour of the vitreous humour was characterized according to a four-parameter Burgers model, consisting

† Email address for correspondence: rodolfo.repetto@unige.it

of a Maxwell element in series with a Kelvin element. In a second paper, Lee, Litt & Buchsbaum (1994) showed that the viscoelastic behaviour of the central region of the porcine vitreous humour closely resembles that of the human. More recently, Nickerson *et al.* (2008) performed rheological measurements of bovine and porcine vitreous humour. They showed that, during the first hour after dissection, the shear modulus of the vitreous humour decreases significantly, eventually reaching a steady-state value. Swindle, Hamilton & Ravi (2008) also observed variation of the rheological properties of porcine vitreous humour with time after dissection. Both Nickerson *et al.* (2008) and Swindle *et al.* (2008) attribute the temporal variation of the properties to mass loss and microstructural changes within the vitreous humour, and state that the vitreous properties *in vivo* should be similar to those they measured in the initial phase of the experiments. The values of the shear moduli obtained by Swindle *et al.* (2008) are lower than those of Nickerson *et al.* (2008), but both are of the same order of magnitude.

During eye rotations, the vitreous humour exerts stresses on the retina that may play a role in the development of a variety of vitreoretinal pathologies, in particular in retinal detachment. This is a serious condition that threatens the sight of the sufferer. The most common type is rhegmatogeneous retinal detachment, which occurs when a tear forms in the retina, allowing fluid to enter the space between the retina and the choroid. The mechanics of retinal tearing and the detachment process are not well understood. An improved understanding of such processes could pave the way to new and more efficient clinical and surgical treatments (Scott 2002).

Very few *in vivo* observations of the motion of the vitreous humour induced by eye rotations are available. Zimmerman (1980) recorded the movement of the scattering pattern induced by a point source of light during the relaxation movement of the vitreous humour following an impulsive eye rotation. According to his measurements, the vitreous humour behaves as an overdamped system that is close to critical damping. Walton *et al.* (2002) used ultrasound films of eyes performing impulsive rotations and tracked the speckles present in the vitreous humour. They observed that the vitreous humour undergoes significant mechanical changes as the age of the patient increases.

One of the first mathematical models of the motion of the vitreous humour induced by eye rotations was due to Buchsbaum *et al.* (1984), who studied the linearized behaviour of a viscoelastic fluid in a sphere performing periodic and impulsive rotations. David *et al.* (1998) developed a similar model, using the mechanical behaviour proposed by Lee *et al.* (1992) to describe the vitreous humour. One of their main findings is that the shear stress at the wall grows more than linearly with the eye radius. They propose this as a possible explanation as to why myopic eyes, which are typically larger than normal ones, have an increased risk of retinal detachment.

The motion of a Newtonian fluid in a spherical cavity performing periodic torsional oscillations has been studied experimentally and theoretically (Repetto, Stocchino & Cafferata 2005; Repetto, Siggers & Stocchino 2008), with the aim of finding the stress on the retina and understanding mixing processes in the vitreous humour, which are relevant for intra-vitreal drug delivery.

In this paper we develop a model to improve the understanding of the stresses exerted on the retina during eye rotations and their relationship to the mechanical properties of the vitreous. We model the vitreous humour as a viscoelastic fluid and the vitreous chamber as a sphere, and consider both the free motion of the fluid and also the motion forced by rotations of the domain.

The paper proceeds as follows. In § 2 we formulate the mathematical model. In § 3 we investigate the flows that are produced during relaxation of the vitreous humour from an initially moving and deformed state. We evaluate the natural frequencies and rates of decay of the motion associated with two simple viscoelastic models: the first using the measurements taken by Nickerson *et al.* (2008) and Swindle *et al.* (2008), and the second being the model proposed by Lee *et al.* (1992). In § 4 we consider the flow driven by periodic, torsional rotations of the sphere, and investigate the possible occurrence of resonant phenomena. Discussion of the results and conclusions follow in § 5.

2. Mathematical formulation

2.1. *Governing equations*

We consider the slow flow of an incompressible viscoelastic fluid of density ρ occupying a spherical region of radius R_0. The governing equations are given by the Cauchy equation and the continuity equation:

$$\rho\left(\frac{\partial \boldsymbol{u}}{\partial t}+\boldsymbol{u}\cdot\boldsymbol{\nabla}\boldsymbol{u}\right)=\boldsymbol{\nabla}\cdot\boldsymbol{\sigma},\quad \boldsymbol{\nabla}\cdot\boldsymbol{u}=0. \tag{2.1a, b}$$

Here $\boldsymbol{u}$ is the velocity, t is time and $\boldsymbol{\sigma}$ is the stress tensor, given by $\boldsymbol{\sigma}=-p\boldsymbol{I}+\boldsymbol{d}$, where p is the pressure, $\boldsymbol{d}$ is the deviatoric part of the stress tensor (which, in a viscoelastic fluid, depends on the history of the fluid motion) and $\boldsymbol{I}$ is the identity matrix. Since we consider slow flow, we linearize in the velocity, and assuming the rheological properties of the fluid to be steady, homogeneous and isotropic and $\boldsymbol{d}$ to be a linear function of the velocity gradients, we can, in general, write (e.g. Tanner 2000)

$$\boldsymbol{d}=2\int_{-\infty}^{t}G\,(t-s)\,\boldsymbol{D}\,(s)\,\mathrm{d}s, \tag{2.2}$$

for some function G, which is the relaxation modulus of the fluid, where

$$\boldsymbol{D}=\tfrac{1}{2}\left(\boldsymbol{\nabla}\boldsymbol{u}+(\boldsymbol{\nabla}\boldsymbol{u})^{\mathrm{T}}\right) \tag{2.3}$$

is the rate-of-deformation tensor. Thus, neglecting quadratic terms in the velocity, (2.1*a*) becomes

$$\rho\frac{\partial \boldsymbol{u}}{\partial t}=-\boldsymbol{\nabla}p+\int_{-\infty}^{t}G\,(t-s)\,\boldsymbol{\nabla}^2\boldsymbol{u}\,\mathrm{d}s. \tag{2.4}$$

No-slip boundary conditions are applied at the wall of the sphere.

2.2. *Eigenfunctions of the system*

The system can be simplified by formulating it as nonlinear eigenvalue problem, and working in terms of the eigenfunctions, $(\boldsymbol{u}_\lambda(\boldsymbol{x}), p_\lambda(\boldsymbol{x}))$, which satisfy (2.1*b*) and (2.4) with constant complex growth rate λ, corresponding to the relaxation time $\tau=1/\mathrm{Re}(\lambda)$. Seeking solutions of the form $\boldsymbol{u}=\boldsymbol{u}_\lambda \mathrm{e}^{\lambda t}+\text{c.c.}$ and $p=p_\lambda \mathrm{e}^{\lambda t}+\text{c.c.}$, where c.c. denotes the complex conjugate, we obtain

$$\rho\lambda\boldsymbol{u}_\lambda=-\boldsymbol{\nabla}p_\lambda+\frac{\tilde{G}(\lambda)}{\lambda}\boldsymbol{\nabla}^2\boldsymbol{u}_\lambda,\quad \boldsymbol{\nabla}\cdot\boldsymbol{u}_\lambda=0, \tag{2.5a, b}$$

where

$$\tilde{G}(\lambda) = \lambda \int_0^\infty G(s)\, \mathrm{e}^{-\lambda s}\, \mathrm{d}s \tag{2.6}$$

is the complex modulus of the fluid, and we also define

$$G'(\lambda) = \mathrm{Re}(\tilde{G}(\lambda)), \quad G''(\lambda) = \mathrm{Im}(\tilde{G}(\lambda)), \tag{2.7a, b}$$

which respectively quantify the elastic and viscous behaviour of the fluid.

We work in spherical coordinates $(\tilde{r}, \theta, \phi)$, where $\tilde{r} = rR_0$, $r \in [0, 1]$, $\theta \in [0, \pi]$ and $\phi \in [0, 2\pi)$, and write the velocity components of the eigenfunctions as a sum of vector spherical harmonics $\mathbb{P}_{mn}(\theta, \phi)$, $\mathbb{B}_{mn}(\theta, \phi)$ and $\mathbb{C}_{mn}(\theta, \phi)$, and the pressures as a sum of scalar spherical harmonics $Y_{mn}(\theta, \phi)$, where $m, n \in \mathbb{Z}$, $n \geqslant 0$ and $-n \leqslant m \leqslant n$ (see the Appendix); thus

$$\begin{aligned} \boldsymbol{u}_\lambda = &\sum_{n=0}^{\infty} \sum_{m=-n}^{n} u_{mn}(r; \lambda)\mathbb{P}_{mn}(\theta, \phi) + v_{mn}(r; \lambda)\mathbb{B}_{mn}(\theta, \phi) \\ &+ w_{mn}(r; \lambda)\mathbb{C}_{mn}(\theta, \phi), \end{aligned} \tag{2.8}$$

$$p_\lambda = \sum_{n=0}^{\infty} \sum_{m=-n}^{n} p_{mn}(r; \lambda) Y_{mn}(\theta, \phi). \tag{2.9}$$

Note that $\mathbb{B}_{00}$ and $\mathbb{C}_{00}$ are identically zero. Imposing regularity conditions at the origin ($r = 0$) implies that we must impose the boundary conditions $\mathrm{d}p_{00}/\mathrm{d}r|_{r=0} = u_{00}|_{r=0} = 0$, $p_{m1}|_{r=0} = w_{m1}|_{r=0} = 0$, $v_{m1}|_{r=0} = \sqrt{2}u_{m1}|_{r=0}$, $\mathrm{d}u_{m1}/\mathrm{d}r|_{r=0} = \mathrm{d}v_{m1}/\mathrm{d}r|_{r=0} = 0$, and also for $n > 1$, $p_{mn}|_{r=0} = u_{mn}|_{r=0} = v_{mn}|_{r=0} = w_{mn}|_{r=0} = 0$. Substituting into (2.5*a*,*b*), making use of standard orthogonality conditions for vector spherical harmonics (see the Appendix and Quartapelle & Verri 1995) and applying the regularity conditions at the origin, we obtain the general solution

$$p_{mn} = -\frac{C^{(1)}_{mn}\lambda}{n} r^n, \tag{2.10a}$$

$$u_{mn} = C^{(1)}_{mn} r^{n-1} + C^{(2)}_{mn} \frac{j_n(ar)}{r}, \tag{2.10b}$$

$$v_{mn} = \frac{C^{(1)}_{mn} s_n}{n} r^{n-1} + C^{(2)}_{mn} \frac{arj_{n-1}(ar) - nj_n(ar)}{s_n r}, \tag{2.10c}$$

$$w_{mn} = C^{(3)}_{mn} j_n(ar), \tag{2.10d}$$

for $n > 0$ and $p_{00} = u_{00} = 0$, where j_n is the nth spherical Bessel function given by $j_n(x) = \sqrt{\pi/(2x)}\mathrm{J}_{n+1/2}(x)$, $s_n = \sqrt{n(n+1)}$, $a = \sqrt{-\rho\lambda^2 R_0^2/\tilde{G}(\lambda)}$ and $C^{(1)}_{mn}$, $C^{(2)}_{mn}$ and $C^{(3)}_{mn}$ are constants to be determined by applying the boundary conditions.

3. Relaxation behaviour

3.1. *Eigenvalues and eigenfunctions of the system*

In this section we investigate the relaxation behaviour of the system, starting from a prescribed non-zero velocity field at $t = 0$ and assuming the eyeball remains stationary for $t > 0$, looking in particular for natural frequencies of oscillation that could be resonantly excited by eye rotations.

Enforcing no-slip boundary conditions on the solution (2.10*a–d*) and seeking a non-trivial solution leads to

$$j_{n+1}(a) = 0 \quad \text{or} \quad j_n(a) = 0. \tag{3.1a, b}$$

The roots of the function j_n are all real, the eigenfunctions corresponding to $-a$ and a are linearly dependent, and the root $a = 0$ does not correspond to an eigenfunction. We define a_{ln} as the lth positive zero of the function $j_n(x)$.

The growth rates are given by the solutions for λ of

$$\lambda = \sqrt{-\frac{\tilde{G}(\lambda)}{\rho R_0^2}}\, a_{ln}. \tag{3.2}$$

Depending on the function $\tilde{G}$, (3.2) could admit several solutions. We denote the number of solutions by Q_{ln} and let the solutions corresponding to a_{ln} be $\lambda_{ln}^{(q)}$, where $q = 1, 2, \ldots, Q_{ln}$; we will show in the next sections that two/four solutions exist in the case that the rheology is described by a two/four-parameter model. The eigenfunctions can be written as

$$\mathscr{V}_{lmn}^{(kq)} = (\boldsymbol{u}_{lmn}^{(kq)}, p_{lmn}^{(kq)}), \tag{3.3}$$

where $k \in \{1, 2\}$, $q \in \{1, 2, \ldots, Q_{ln}\}$, $l \in \mathbb{N}$, $m \in \mathbb{Z}$, and, if $k = 1$ then $n \in \mathbb{N}\backslash\{1\}$ and $|m| \leqslant n - 1$, whereas if $k = 2$, $n \in \mathbb{N}$ and $|m| \leqslant n$. The solutions fall into two categories: type 1 eigenfunctions ($k = 1$), given by

$$\begin{aligned}\boldsymbol{u}_{lmn}^{(1q)} = &\left(\frac{j_{n-1}(a_{ln}r)}{r j_{n-1}(a_{ln})} - r^{n-2}\right)\mathbb{P}_{mn-1} \\ &+ \left(\frac{a_{ln} r j_{n-2}(a_{ln}r) - (n-1) j_{n-1}(a_{ln}r)}{s_{n-1} r j_{n-1}(a_{ln})} - \frac{n}{s_{n-1}} r^{n-2}\right)\mathbb{B}_{mn-1},\end{aligned} \tag{3.4}$$

$$p_{lmn}^{(1q)} = \frac{\lambda_{ln}^{(q)}}{n-1} r^{n-1} Y_{mn-1}, \tag{3.5}$$

and type 2 eigenfunctions ($k = 2$),

$$\boldsymbol{u}_{lmn}^{(2q)} = j_n(a_{ln}r)\mathbb{C}_{mn}, \tag{3.6}$$

$$p_{lmn}^{(2q)} = 0. \tag{3.7}$$

For the sake of clarity we recall the meaning of all indices appearing in expressions (3.1)–(3.7): m and n refer to the mode of the spherical harmonic expansions (2.8) and (2.9), l denotes the lth radial mode (lth zero of the function $j_n(x)$), k differentiates between the two categories of eigenfunctions, and finally q identifies the qth solution of (3.2). Note that, although we have denoted the eigenfunctions $\boldsymbol{u}_{lmn}^{(kq)}$ and $p_{lmn}^{(kq)}$, of these functions only $p_{lmn}^{(1q)}$ depends on the value of q. Note also that the growth rates $\lambda_{ln}^{(q)}$ are independent of both the type of eigenfunction, k, and of the azimuthal wavenumber, m. In the Appendix, we show that the fact that the eigenvalues $\lambda_{ln}^{(q)}$ do not depend on the azimuthal wavenumber, m, is a consequence of the spherical symmetry of the system. In particular, we show that an eigenfunction, $\mathscr{V}_{lmn}^{(kq)}$, in a rotated coordinate system can be expressed as a linear combination of eigenfunctions with the same value of the indices k, q, l and n. Moreover, for a given m_0, every eigenfunction, $\mathscr{V}_{lmn}^{(kq)}$, can be written as a linear superposition of rotations of the

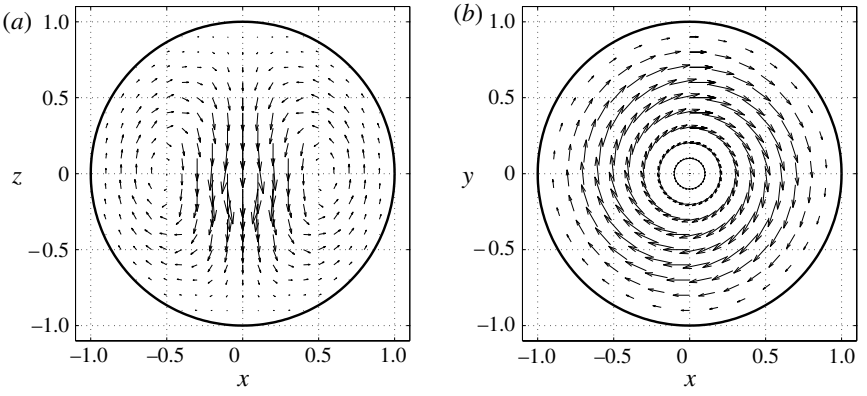

FIGURE 1. Spatial structure of the eigenfunctions (*a*) $\boldsymbol{u}_{102}^{(1q)}$ and (*b*) $\boldsymbol{u}_{101}^{(2q)}$ on the planes $\phi = 0, \pi$ (x–z plane) and $\theta = \pi/2$ (x–y plane), respectively.

eigenfunction $\mathscr{V}_{lm_0n}^{(kq)}$. This indicates that, for a given growth rate $\lambda_{ln}^{(q)}$, there are two distinct sets of eigenfunctions sharing the same eigenvalue, $\{\mathscr{V}_{lmn}^{(1q)} : |m| \leqslant n-1\}$ and $\{\mathscr{V}_{lmn}^{(2q)} : |m| \leqslant n\}$, such that, within each set, all the elements are related by rotations.

The eigenfunctions form a complete set, and therefore the solution of (2.5*a*,*b*) can be written in the form

$$\boldsymbol{u} = \sum_{n=1}^{\infty}\sum_{m=-n}^{n}\sum_{l=1}^{\infty}\sum_{k=1}^{2}\sum_{q=1}^{Q_{ln}} A_{lmn}^{(kq)}\boldsymbol{u}_{lmn}^{(kq)}(r,\theta,\phi)\mathrm{e}^{\lambda_{ln}^{(q)}t} + \text{c.c.}, \tag{3.8a}$$

$$p = \sum_{n=1}^{\infty}\sum_{m=-n}^{n}\sum_{l=1}^{\infty}\sum_{k=1}^{2}\sum_{q=1}^{Q_{ln}} A_{lmn}^{(kq)}p_{lmn}^{(kq)}(r,\theta,\phi)\mathrm{e}^{\lambda_{ln}^{(q)}t} + \text{c.c.}, \tag{3.8b}$$

where $A_{lmn}^{(kq)}$ are constants that can be found from the initial conditions (note that $\mathscr{V}_{l,\pm n,n}^{(1q)}$ and $\mathscr{V}_{l01}^{(1q)}$ are zero). The number of initial conditions needed is equal to Q_{ln}. It can be shown that, in the case of a Newtonian fluid, $Q_{ln} = 1$, so one initial condition (the velocity field) is needed; whereas, in the case of an elastic solid, $Q_{ln} = 2$, so two initial conditions (the initial deformation and the velocity field) are needed. By way of example, we show the spatial structure of the eigenfunctions $\boldsymbol{u}_{102}^{(1q)}$ and $\boldsymbol{u}_{101}^{(2q)}$ in figures 1(*a*) and 1(*b*), respectively.

3.2. *Two-parameter model of the viscoelastic behaviour*

Nickerson *et al.* (2008) and Swindle *et al.* (2008) performed experiments on a porcine model with angular frequencies $\omega = 10.0$ rad s^{-1} and $\omega = 12.6$ rad s^{-1} to obtain the complex modulus of the fluid. To formulate a model of the shear behaviour, we must make an assumption about the dependence of the rheology upon the frequency. We assume that the shear behaviour can be represented by a Kelvin element (e.g. Tanner 2000) consisting of an ideal dashpot (a viscous element) with constant η_K connected in parallel with an ideal spring (an elastic element) with constant μ_K. In this case the complex modulus is given by the sum of the moduli of the elements, which can be found from (2.6), and equals

$$\tilde{G}(\lambda) = \mu_K + \lambda\eta_K. \tag{3.9}$$

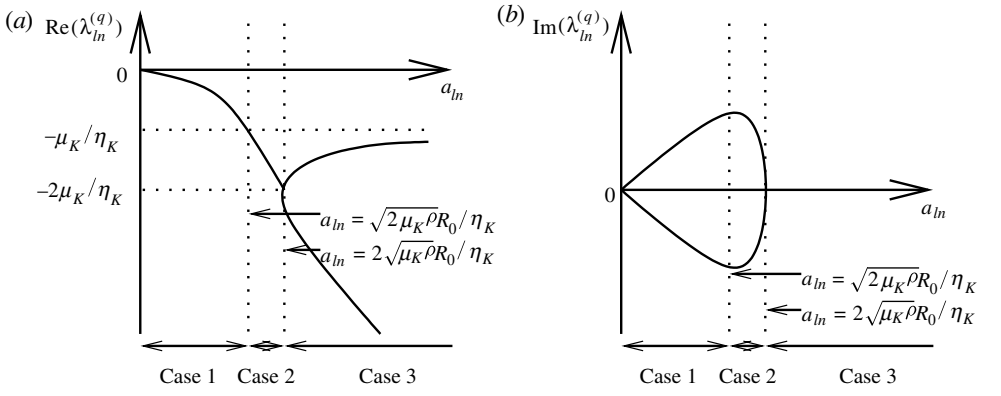

FIGURE 2. Sketch of the (*a*) real and (*b*) imaginary parts of the growth rates $\lambda_{ln}^{(q)}$ as a function of a_{ln} for the two-parameter model described in § 3.2. Note that the roots are ordered $a_{11} < a_{12} < a_{13} < a_{21} < \cdots$.

The complex moduli measured by Nickerson *et al.* (2008) and Swindle *et al.* (2008) and the corresponding values of μ_K and η_K are listed in table 1. In figure 4 of Nickerson *et al.* (2008), measured values of G' and G'' are presented in an experiment in which the vitreous humour undergoes periodic forced oscillations at different frequencies. At each frequency, the oscillations continue for sufficiently long that transients decay before the measurements are taken. If the two-parameter model were faithful, then $G' = \mu_K$ should be constant and $G'' = \omega\eta_K$ should increase linearly with increasing rotation frequency. The comparison with figure 4 of Nickerson *et al.* (2008) reveals this model to be far from perfect, but, in the absence of more extensive experimental work, we consider the Kelvin element. We will discuss the data from Nickerson *et al.*'s figure 4, and the qualitative behaviour of the model more extensively in § 4.2.

Equations (3.2) and (3.9) lead to a quadratic equation with solutions

$$\lambda_{ln}^{(1)} = -\frac{\eta_K a_{ln}^2}{2\rho R_0^2} + \sqrt{\frac{\eta_K^2 a_{ln}^4}{4\rho^2 R_0^4} - \frac{\mu_K a_{ln}^2}{\rho R_0^2}}, \tag{3.10a}$$

$$\lambda_{ln}^{(2)} = -\frac{\eta_K a_{ln}^2}{2\rho R_0^2} - \sqrt{\frac{\eta_K^2 a_{ln}^4}{4\rho^2 R_0^4} - \frac{\mu_K a_{ln}^2}{\rho R_0^2}}. \tag{3.10b}$$

The real parts of $\lambda_{ln}^{(q)}$ are negative, which confirms the system's dissipative nature. Figure 2 shows a sketch of the real and imaginary parts of $\lambda_{ln}^{(q)}$ plotted against the root a_{ln}. The flow can be written as a linear superposition of the eigenfunctions, each multiplied by a time-dependent coefficient that decays with rate constant equal to the real part of the corresponding eigenvalue. At long times, therefore, the flow will be a superposition of those eigenfunctions whose eigenvalues have largest real part. Inspecting figure 2, for each l and n, we can distinguish three cases corresponding to each of the roots a_{ln}.

(i) Case 1, $a_{ln} < \sqrt{2\mu_K\rho}R_0/\eta_K$: the eigenvalues $\lambda_{ln}^{(q)}$ are a complex conjugate pair with a negative real part that is larger than the real parts of all but a finite number of the other eigenvalues. Hence the amplitude of the corresponding eigenfunction is oscillatory and decaying, but it has a slower decay than that of all but a finite

https://doi.org/10.1017/jfm.2011.263 Published online by Cambridge University Press

	G' (Pa)	G'' (Pa)	μ_K (Pa)	η_K (Pa s)	$\lambda_{11}^{(q)}$ $(q = 1, 2)$ (rad s^{-1})	Case (1, 2 or 3)	Slowest decay (rad s^{-1})
[N] IV	10	3.9	10	0.39	-27.20 ± 25.59i	2	-25.64
[N] FV	2.8	0.7	2.8	0.07	-4.88 ± 19.15i	1	-4.88
[S] IV	3.46	0.71	3.46	0.056	-3.94 ± 21.61i	1	-3.94
[S] FV	0.64	0.37	0.64	0.03	-2.05 ± 9.22i	1	-2.05

TABLE 1. Values of the complex modulus (G' and G'') measured by Nickerson *et al.* (2008) [N] (using an angular frequency of 10 s^{-1}) and Swindle *et al.* (2008) [S] (using an angular frequency of 12.57 s^{-1}). Corresponding calculated parameters shown are the spring (μ_K) and dashpot (η_K) parameters, the first eigenvalue $\lambda_{11}^{(q)}$, the case in which it falls (see text) and the slowest decay rate (largest real part of all the eigenvalues). The parameter values used are $\rho = 1005.3$ kg m^{-3} and $R_0 = 0.012$ m, and IV and FV, respectively, denote initial and final values in the experiments.

number of the other eigenfunctions. If the smallest root, a_{11}, falls in case 1 (true for the final values of Nickerson *et al.* (2008) and both initial and final values of Swindle *et al.* (2008), see table 1) then, assuming that at least one of the eigenfunctions $\mathscr{V}_{1m1}^{(2q)}$ was excited at $t = 0$, the overall system is underdamped, and the profile at long times will be a superposition of the eigenfunctions $\mathscr{V}_{1m1}^{(2q)}$. The presence of natural frequencies leads to the possibility of resonant excitation during forced oscillations, and this will be discussed in the second part of this paper.

(ii) Case 2, $\sqrt{2\mu_K\rho}R_0/\eta_K < a_{ln} < 2\sqrt{\mu_K\rho}R_0/\eta_K$: the eigenvalues $\lambda_{ln}^{(q)}$ are also a complex conjugate pair with negative real part, and so, as in case 1, the amplitude of the corresponding eigenfunction is oscillatory and decaying. However, in this case there are infinitely many other eigenvalues $\lambda_{l'n'}^{(q)}$ with larger real parts. These are any eigenvalues for which $a_{l'n'} < a_{ln}$, as well as those with sufficiently large values of l' or n'. In particular, if the smallest root a_{11} falls in case 2 (true for the initial values of Nickerson *et al.* (2008), see table 1), and assuming that at least one eigenfunction with a_{ln} sufficiently large was excited at $t = 0$, the overall system is overdamped, and the long-time behaviour is a superposition of eigenfunctions $\mathscr{V}_{lmn}^{(kq)}$ with large l or n whose amplitude decays exponentially in time. However, for typical initial conditions, the coefficients multiplying the eigenfunctions corresponding to the largest values of a_{ln} are likely to be very small, and hence very long times must be reached before the dominant flow corresponds to these eigenfunctions. This case also does not exclude the possibility of resonance excited by forced oscillations.

(iii) Case 3, $a_{ln} > 2\sqrt{\mu_K\rho}R_0/\eta_K$: the eigenvalues $\lambda_{ln}^{(q)}$ are real, and so the corresponding eigenfunction decays exponentially with time. As in case 2 there are infinitely many eigenfunctions with a slower decay, which are those corresponding to larger values of $a_{l'n'}$. If a_{11} is as in case 3, then the overall system is overdamped. In this case there are no natural frequencies present in the system, so we do not expect resonance.

In figure 3 we show curves in the (μ_K, η_K) plane separating the three cases. Both decreasing the viscosity η_K and increasing the elastic constant μ_K leads to an increase in the number of modes with complex eigenvalues. The parameter values measured by Nickerson *et al.* (2008) and Swindle *et al.* (2008) are also indicated in the figure, which shows that, for all the measured parameters the model predicts the existence of some roots in cases 1 and 2, implying that the corresponding eigenfunctions will possess natural frequencies. Note, however, that the system is not far from critical damping, and, specifically for the initial values measured by Nickerson *et al.* (2008), only the modes $\mathscr{V}_{1m1}^{2q}$, $\mathscr{V}_{1m2}^{2q}$ and $\mathscr{V}_{1m2}^{1q}$ for $q = 1, 2$ correspond to a complex eigenvalue and thus admit the possibility of resonance.

3.3. *Four-parameter model of the viscoelastic behaviour*

The vitreous humour has also been described using a Burgers model, consisting of a Kelvin element in series with a dashpot and a spring (Lee *et al.* 1992). The moduli of elements add when connected in parallel and their compliances add when connected in series. Using (2.6), the complex modulus can be written in terms of the moduli of the components as

$$\tilde{G}(\lambda) = \left(\frac{1}{\mu_K + \lambda\eta_K} + \frac{1}{\mu_M} + \frac{1}{\lambda\eta_M} \right)^{-1}. \tag{3.11}$$

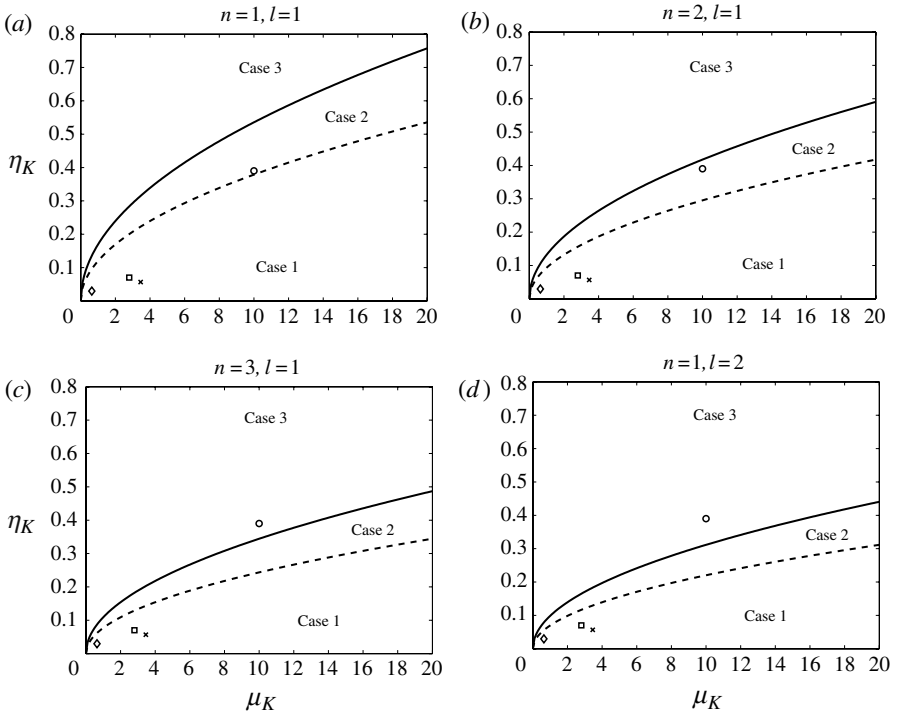

FIGURE 3. The curves show the boundaries in the (μ_K, η_K) plane between cases 1, 2 and 3 (described in the text) for the eigenfunctions corresponding to the smallest four values of a_{ln}, as follows: (*a*) $l = 1$, $n = 1$ (corresponding to $\mathscr{V}^{(2q)}_{1m1}$, $m = -1, 0, 1$); (*b*) $l = 1$, $n = 2$ (corresponding to $\mathscr{V}^{(kq)}_{1m2}$, $k = 1$ and $m = -1, 0, 1$, or $k = 2$ and $m = -2, -1, 0, 1, 2$); (*c*) $l = 1$, $n = 3$ (corresponding to $\mathscr{V}^{(kq)}_{1m3}$, $k = 1$ and $m = -2, -1, 0, 1, 2$, or $k = 2$ and $m = -3, -2, -1, 0, 1, 2, 3$); and (*d*) $l = 2$, $n = 1$ (corresponding to $\mathscr{V}^{(2q)}_{2m1}$, $m = -1, 0, 1$). The symbols show values measured experimentally, as follows: circle, Nickerson *et al.* (2008), initial values; square, Nickerson *et al.* (2008), final values; cross, Swindle *et al.* (2008), initial values; diamond, Swindle *et al.* (2008), final values.

Parameter	Anterior	Central	Posterior
μ_K (Pa)	2.5	1.27	1.21
μ_M (Pa)	3.67	7.27	3.01
η_M (Pa s)	1.398	2.18	4.86
η_K (Pa s)	0.313	0.352	0.49

TABLE 2. Measured values of the moduli of the elements of the Burgers model in three different locations in the eye. Taken from Lee *et al.* (1992).

Substituting this expression into (3.2) yields a third-order polynomial equation for λ. It can be shown that the real parts of all the roots are always negative.

Experimentally measured values of the moduli of the elements are given in table 2. There is a transition point a_* such that eigenfunctions with $a_{ln} \leqslant a_*$ have all four growth rates real, and thus their decay is overdamped. For $a_{ln} > a_*$ there are two real

and two complex growth rates. For the measured parameter values in table 2, a_* is sufficiently small that all cases have two real and two complex roots. As $l \to \infty$ the imaginary part of the complex conjugate pair tends to infinity, while the real part tends to a constant. Adopting the values proposed by Lee *et al.* (1992) for the anterior vitreous humour, the eigenvalue with the largest real part is complex, whereas, with the values proposed for the central and posterior vitreous humour, the eigenvalue with the largest real part is real.

4. Behaviour under periodic forcing

4.1. *Calculation of the flow and kinetic energy*

We now study how the vitreous humour responds to eye rotations. For simplicity we consider small-amplitude sinusoidal torsional oscillations of angular displacement $\beta(t) = -\epsilon \cos \omega_0 t$. Mathematically, this is now a forced problem in which, contrary to the eigenvalue problem discussed in the previous part of the paper, the boundary conditions are non-homogeneous and read

$$\boldsymbol{u} = \epsilon \omega_0 R_0 \sin\theta \sin \omega_0 t \, \hat{\boldsymbol{\phi}}, \tag{4.1}$$

where $\hat{\boldsymbol{\phi}}$ is the unit vector in the azimuthal direction. The assumption of small-amplitude eye movements allows us to linearize the problem. Of course, real eye rotations are not truly periodic; however, the experiments performed by Repetto *et al.* (2005) with purely Newtonian fluids indicate that, starting from rest, the motion is very close to periodic after only a few rotations of the domain. Thus when the eye is performing a repetitive motion, even for only a small number of saccades, we anticipate that the flow will be close to the solution of the idealized system with periodic forcing.

We seek periodic solutions of the governing equations, corresponding to long times. Since all the eigenfunctions decay, at long times the solution is approximately periodic with frequency ω_0. Expanding the velocity and pressure as a sum of spherical harmonics and assuming periodicity, the velocity and pressure fields are given by (2.8) and (2.9), where

$$p_{mn} = -\frac{C^{(1)}_{mn} \mathrm{i}\omega_0}{n} r^n, \tag{4.2a}$$

$$u_{mn} = C^{(1)}_{mn} r^{n-1} + C^{(2)}_{mn} \frac{j_n(ar)}{r}, \tag{4.2b}$$

$$v_{mn} = \frac{C^{(1)}_{mn} s_n}{n} r^{n-1} + C^{(2)}_{mn} \frac{arj_{n-1}(ar) - nj_n(ar)}{s_n r}, \tag{4.2c}$$

$$w_{mn} = C^{(3)}_{mn} j_n(ar), \tag{4.2d}$$

with

$$a = \alpha_c \mathrm{e}^{-\mathrm{i}\pi/4}, \quad \alpha_c = \sqrt{\frac{\rho \omega_0 R_0^2}{\tilde{G}(\mathrm{i}\omega_0)/(\mathrm{i}\omega_0)}}, \tag{4.3}$$

where α_c is the complex Womersley number. Applying the boundary conditions, only $C^{(3)}_{01}$ can be non-zero; an example is illustrated in figure 1(*b*), and we obtain the

velocity and pressure fields

$$\boldsymbol{u} = \sqrt{\frac{\pi}{3}}\frac{\epsilon R_0\omega_0 j_1(ar)}{\mathrm{i}j_1(a)}\mathrm{e}^{\mathrm{i}\omega t}\mathbb{C}_{01} + \text{c.c.}, \quad p = 0, \tag{4.4}$$

or, with u_r, u_θ and u_ϕ respectively denoting the r, θ and ϕ components of the velocity,

$$\begin{aligned} u_\phi &= \frac{\epsilon R_0\omega_0 j_1(ar)}{2\mathrm{i}j_1(a)}\sin\theta\,\mathrm{e}^{\mathrm{i}\omega_0 t} + \text{c.c.} \\ &= -\frac{\mathrm{i}\epsilon R_0\omega_0(\sin ar - ar\cos ar)}{2r^2(\sin a - a\cos a)}\sin\theta\,\mathrm{e}^{\mathrm{i}\omega_0 t} + \text{c.c.} \end{aligned} \tag{4.5}$$

and $u_r = u_\theta = p = 0$, after David *et al.* (1998).

For the following discussion it is useful to introduce the total kinetic energy of the fluid, $\mathscr{K}$, which, at leading order, is given by

$$\mathscr{K} = \frac{1}{2}\int_{sphere}\rho\,|\boldsymbol{u}|^2\,\mathrm{d}V = \frac{4\pi}{3}\rho R_0^5\omega_0^2\epsilon^2\int_0^1\left(\frac{j_1(ar)}{2\mathrm{i}j_1(a)}\mathrm{e}^{\mathrm{i}\omega_0 t} + \text{c.c.}\right)^2 r^2\,\mathrm{d}r. \tag{4.6}$$

The time average of the kinetic energy over a cycle equals

$$\overline{\mathscr{K}} = \frac{2\pi}{3}\rho R_0^5\omega_0^2\epsilon^2\int_0^1\left|\frac{j_1(ar)}{j_1(a)}\right|^2 r^2\,\mathrm{d}r. \tag{4.7}$$

The stress exerted by this flow on the surface of the sphere is in the azimuthal direction and equals

$$\frac{\epsilon}{2}\left(\frac{a^2}{1 - a\cot a} - 3\right)\tilde{G}(i\omega_0)\sin\theta\,\mathrm{e}^{\mathrm{i}\omega_0 t} + \text{c.c.} \tag{4.8}$$

4.2. *Results*

We first consider a general function $\tilde{G}$, and in figure 4 we show the logarithm of the normalized time-averaged kinetic energy of the system, $\overline{\mathscr{K}}^*$, which is the time-averaged kinetic energy $\overline{\mathscr{K}}$ of the fluid divided by the kinetic energy of a rigid sphere with the same density as the fluid, which is $(2/15)\pi\rho R_0^5\omega_0^2\epsilon^2$. High values of this quantity indicate the possible occurrence of resonant excitation of the vitreous motion. This is shown in the complex a plane. The locations of the wavenumbers $a_{ln} \in \mathbb{R}$ in the plane are also shown by the white symbols. In a viscous fluid (imaginary axis of figure 4), $\overline{\mathscr{K}}^* \leqslant 1$, and $\overline{\mathscr{K}}^* \to 1$ as $\alpha \to 0$, where α is the (real) Womersley number, and $\overline{\mathscr{K}}^* \to 0$ as $\alpha \to \infty$. The other limiting case is that of an elastic non-dissipative solid (real axis in the figure). In this case, the system displays an infinite response ($\overline{\mathscr{K}}^* \to \infty$) at particular forcing frequencies that correspond to some of its eigenfrequencies. Note that only the eigenfunctions $\mathscr{V}_{lmn}^{(kq)}$ with $m = 0$ and $n = 1$ can be resonantly excited by torsional oscillations, which is a result of the fact that the non-homogeneous boundary condition on the azimuthal component of the velocity is proportional to the spherical harmonic with $m = 0$ and $n = 1$.

For a fixed choice of constants for the springs and dashpots, but for different frequencies, the two- and four-parameter models can be represented as curves in the complex a plane. These are shown in figure 4 with different line types representing the different constants measured by Nickerson *et al.* (2008) and Swindle *et al.* (2008) (two-parameter model) and by Lee *et al.* (1992) (four-parameter model).

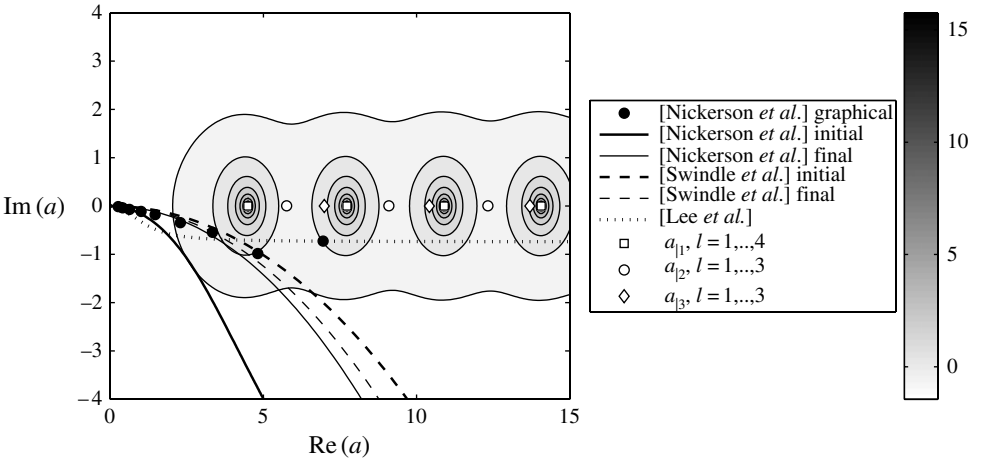

FIGURE 4. Contour plot of the logarithm of the normalized kinetic energy $\overline{\mathscr{K}}^*$ in the complex a plane. The black solid circles show values of a predicted in the experiments of Nickerson *et al.* (2008). Five additional curves showing the values of a over a range of frequencies are plotted. The solid and dashed curves correspond to the two-parameter model, and these use the average values of the parameters μ_K and η_K that are estimated by Nickerson *et al.* (2008) (solid) and Swindle *et al.* (2008) (dashed). The dotted curve shows the values of a obtained using the four-parameter model with parameters estimated by Lee *et al.* (1992).

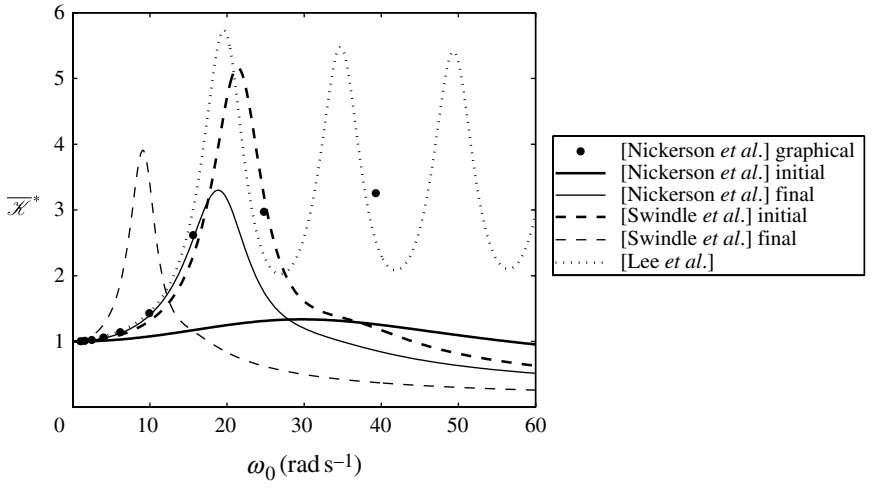

FIGURE 5. Plots of the normalized kinetic energy $\overline{\mathscr{K}}^*$ against frequency. The curves correspond to those described in figure 4.

For frequencies of oscillation corresponding to points at which the curve passes close to one of the singularities of the function $\overline{\mathscr{K}}^*$, the response of the system is expected to be intense.

In the case of the two-parameter model, with the exception of the initial data proposed by Nickerson *et al.* (2008), the curves pass quite close to the first singularity, which corresponds to the excitation of the mode with $l = n = 1$ and $m = 0$, which is

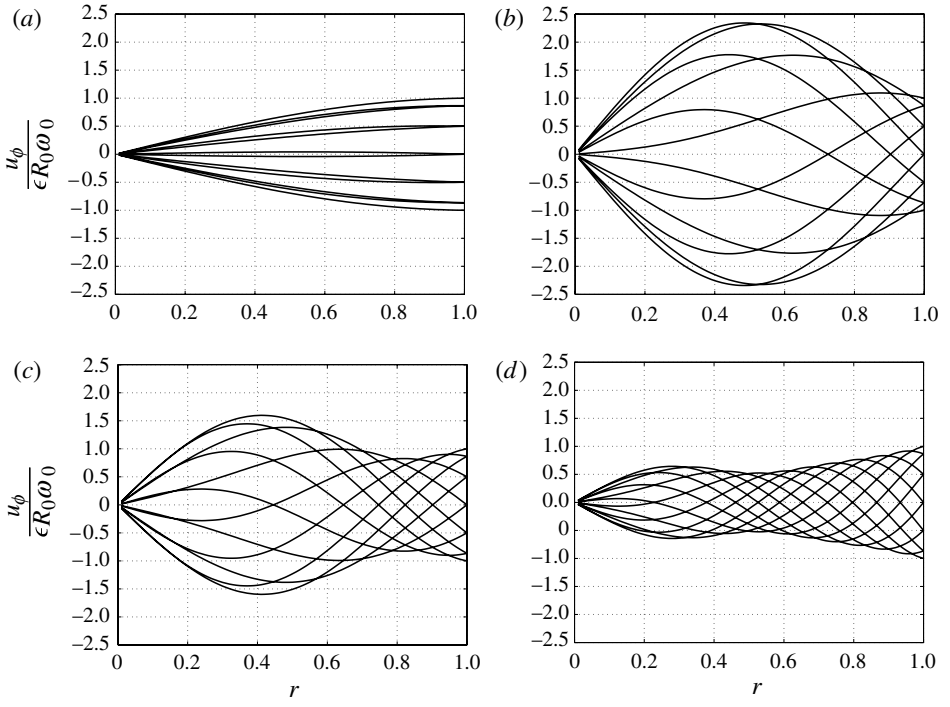

FIGURE 6. Azimuthal velocity profile using the initial values of Swindle *et al.* (2008): (*a*) $\omega = 10$ rad s^{-1}, (*b*) $\omega = 21.61$ rad s^{-1}, (*c*) $\omega = 28$ rad s^{-1} and (*d*) $\omega = 45$ rad s^{-1}. The individual curves show the instantaneous velocity profiles at different times, equally spaced over the period of oscillation.

shown in figure 1(*b*). We plot the normalized kinetic energy in figure 5, which reveals the forcing frequencies ω_0 at which the corresponding peak of the kinetic energy, $\overline{\mathscr{K}}^*$, is observed. The resonant frequencies vary from approximately 10 rad s^{-1} (Swindle *et al.* 2008, final values) to approximately 30 rad s^{-1} (Nickerson *et al.* 2008, initial values). This range of frequencies represents part of the typical range for saccadic eye rotations (e.g. Dyson *et al.* 2004). In spite of the significant damping, the kinetic energy at resonance can be up to approximately six times higher than that of a solid sphere oscillating at the same frequency and amplitude. In figure 4 we also mark the points measured by Nickerson *et al.* (2008) in figure 4 of their paper with solid black circles. With the exception of the last point, the curve traced by the points in the complex a plane has a shape similar to those for the two-parameter model.

As expected following the discussion reported in § 3.3, the situation is markedly different if the four-parameter model is employed. In the complex a plane, the curve for this model tends asymptotically towards the line $\mathrm{Im}(a) = R_0\sqrt{\rho\mu_M}(\eta_K^{-1} + \eta_M^{-1})/2$; see figure 4. Thus an infinite number of modes are excited as the frequency increases, which is also shown in figure 5 by the peaks in excitation.

The radial profiles of the azimuthal velocity are also significantly affected by the frequency of oscillation and, in particular, by the proximity of the forcing frequency to the eigenfrequencies $\mathrm{Im}(\lambda_{l1}^{(q)})$ of the system. In figures 6(*a–d*) we show dimensionless velocity profiles (scaled with the maximum velocity at the boundary) for forcing frequencies (*a*) smaller, (*b*) equal and (*c*,*d*) larger than the natural frequency of the

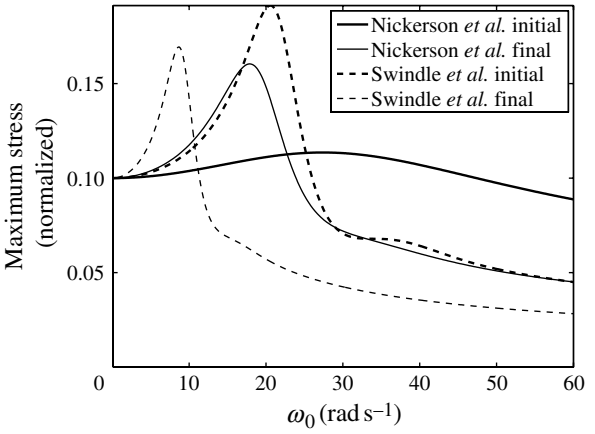

FIGURE 7. Maximum stress at the wall for different forcing frequencies, normalized with $\epsilon\rho R_0^2\omega_0^2$), using data from the papers by Nickerson *et al.* (2008) and Swindle *et al.* (2008).

mode $l = n = 1$, $m = 0$. The curves are obtained using the two-parameter model with the initial data from Swindle *et al.* (2008). These are based on the model corresponding to the curve that passes closest to the singularity of the function $\overline{\mathscr{K}}^*$ at $a = a_{11}$ in figure 4. As expected, for small frequencies of oscillation, figure 6(*a*), the velocity profiles are almost linear. At the resonant frequency, figure 6(*b*), excitation is apparent, and the maximum dimensionless velocity, which occurs near $r = 0.5$, is more than twice as large as the maximum velocity of the boundary. For larger frequencies, figures 6(*c*,*d*), the maximum dimensionless velocity decreases and moves towards the centre of the sphere, which is probably due to a weak excitation of other eigenfunctions.

For the other parameter values measured by Nickerson *et al.* (2008) and Swindle *et al.* (2008), the corresponding curve in the complex a plane is further from the singularities of the function $\overline{\mathscr{K}}^*$. Thus the resonant excitation is not obvious in the velocity profiles, and the profiles are more similar to those found by David *et al.* (1998).

In figure 7 we show plots of the normalized maximum stress versus the forcing frequency. All four plots show a marked maximum stress at the resonant frequency (the imaginary part of $\lambda_{11}^{(q)}$, see table 1). In addition, the initial data of Swindle *et al.* (2008) show a second peak, corresponding to $\lambda_{12}^{(q)}$.

5. Discussion and conclusions

Our motivation is to improve understanding of the motion of the vitreous humour in the vitreous chamber induced by eye rotations. The stress induced by the calculated flows may be related to the occurrence of retinal breaks and detachment. We used measurements of the rheological properties of the vitreous humour available in the literature by Lee *et al.* (1992), who described the vitreous humour using a four-parameter Burgers model, and by Nickerson *et al.* (2008) and Swindle *et al.* (2008), who performed oscillatory tests and provided values for the complex modulus of the fluid. For the latter two we employed a two-parameter Kelvin model to describe the rheological properties; the parameters are the viscosity η_K and the elastic parameter μ_K of the fluid.

In the first part of this paper we studied the eigenvalues and eigenmodes of a viscoelastic fluid within a rigid sphere. The eigenfunctions can be grouped into sets of eigenvectors sharing common properties. For each $k \in \{1, 2\}$, $l \in \mathbb{N}$ and $n \in \mathbb{N}$, any two eigenfunction elements of the set $\{\mathscr{V}_{lmn}^{(kq)} : m \in \mathbb{Z}, |m| \leqslant n, q \in \{1, 2, \ldots, Q_{ln}\}\}$ can be related to one another by rotations. That is, the first eigenfunction can be written as an integral of different rotations of the second.

In all cases corresponding to experimentally measured parameters, we find complex eigenvalues of the system, meaning that there are natural frequencies of oscillation that could be resonantly excited by eye rotations. The natural frequency of the mode with the slowest damping is always approximately in the range 10–25 rad s^{-1}, which is typical of eye rotations.

The two- and four-parameter models lead to qualitatively different results. With the former model we find that only finitely many eigenfunctions have a complex eigenvalue and all the other eigenvalues are real and negative. On the other hand, the latter model predicts an infinite number of modes with complex eigenvalues. The significant differences in the behaviour of the system predicted are intrinsic to the models and do not depend on the particular parameters used.

In the second part of the paper we studied the response of the system to torsional, small-amplitude, sinusoidal oscillations of the sphere. The results show that, when the system is close to resonant excitation, the velocity profiles also display resonance and are qualitatively significantly different from those reported by previous authors (David *et al.* 1998). In particular the maximum velocity can be as much as twice the maximum wall velocity. The resonance generates larger wall shear stresses, and could be relevant for the occurrence of retinal detachment.

Repetto, Siggers & Stocchino (2010) showed that, in the case of a Newtonian fluid, a weak departure of the domain from the spherical shape significantly affects the fluid motion. Their analysis can be extended to the eigenvalue problem considered here, in order to find the effect of a geometrical perturbation on the eigenvalues and eigenfunctions. A small departure from sphericity would induce correspondingly small changes in the eigenvalues of the system from those found in the present model, and therefore, for finite, but sufficiently small, shape perturbations, our predictions of possible resonant excitations of the fluid would still apply.

Measurements of vitreous motion are limited, and we do not know of reports of experimental observations of free oscillations of the vitreous humour in the literature. Zimmerman (1980) described the vitreous humour as an overdamped system, very close to critical damping, and our two-parameter model also predicts that the system is quite close to critical damping. Walton *et al.* (2002) described the motion of the vitreous humour following a single eye rotation, although they do not conclude whether the system possesses natural frequencies. Since the different measurements of the properties of the vitreous humour in the literature lead to a large amount of discrepancy in the theoretical predictions of our model, and there are currently very few *in vivo* observations of vitreous motion, further experimental work is needed.

Another important application of this work is the identification of optimal characteristics for vitreous humour replacement fluids. Soman & Banerjee (2003) and Swindle & Ravi (2007) review all materials currently in use, discuss their advantages and disadvantages, and list the characteristics of an ideal vitreous humour replacement. A common suggestion is that vitreous humour replacements should be viscoelastic fluids with a large enough elastic component to avoid excessive flow within the vitreous chamber (see also Dalton *et al.* 1995). However, they do not account for

the possibility of resonance induced by eye rotations. In fact, using the data for cross-linked hydrogels found both by Swindle-Reilly *et al.* (2009) and by Leone *et al.* (2010) in our two-parameter model, we predict possible resonant excitations. Therefore, in order to avoid high stresses on the retina, our results suggest that it is important to use a material that is well damped, which would prevent strong resonant excitations.

The authors are grateful for the support of the 'British–Italian Partnership Programme' by MIUR-CRUI/British Council, which enabled this work to be carried out.

Appendix. The eigenfunctions of the system and relationships between them

In this section we describe the vector spherical harmonics and their behaviour under rotations, which enables us to relate the eigenfunctions of the system to one another.

Definition of the spherical harmonics

The scalar spherical harmonics Y_{mn} are defined (e.g. Arfken & Weber 2001) as

$$Y_{mn}(\theta,\phi) = (-1)^m \sqrt{\frac{2n+1}{4\pi}\frac{(n-m)!}{(n+m)!}} P_{mn}(\cos\theta)\,\mathrm{e}^{\mathrm{i}m\phi}, \tag{A 1}$$

where $|m| \leqslant n$ and

$$P_{mn}(x) = \begin{cases} 1-x^{2^{m/2}}\left(\dfrac{\mathrm{d}}{\mathrm{d}x}\right)^m P_n(x) & \text{for } m \geqslant 0, \\ (-1)^{|m|}\dfrac{(n-|m|)!}{(n+|m|)!}P_{|m|n}(x) & \text{for } m < 0, \end{cases} \tag{A 2}$$

and P_n is the Legendre polynomial of order n, which has the same parity (odd or even) as n. The functions Y_{mn} are pairwise orthogonal in the sense that $\langle Y_{mn}(\theta,\phi)Y_{m'n'}(\theta,\phi)\rangle = \delta_{mm'}\delta_{nn'}$ where $\langle\cdot$ denotes the integral over the surface of the unit sphere and δ_{ij} is the Kronecker delta function.

The vector spherical harmonics $\mathbb{P}_{mn}(\theta,\phi)$, $\mathbb{B}_{mn}(\theta,\phi)$ and $\mathbb{C}_{mn}(\theta,\phi)$ are defined as

$$\mathbb{P}_{mn} = Y_{mn}\hat{\boldsymbol{r}}, \quad \mathbb{B}_{mn} = \frac{r}{s_n}\boldsymbol{\nabla}Y_{mn}, \quad \mathbb{C}_{mn} = \frac{1}{s_n}\boldsymbol{\nabla}\times(Y_{mn}\boldsymbol{r}), \tag{A 3}$$

where $\boldsymbol{r}$ represents the position vector, $\hat{\boldsymbol{r}}$ the unit vector in the same direction and $s_n = \sqrt{n(n+1)}$. The vector spherical harmonics are pairwise orthogonal in the sense that integration over the surface of the unit sphere of the scalar product of any two of these basis functions equals zero unless the functions are the same, in which case it equals one.

A general rotation of the spherical coordinate system

In this section we find formulae relating two different spherical coordinate systems sharing a common origin. We denote the systems as $\mathscr{C}$ with coordinates (r,θ,ϕ) and $\mathscr{C}'$ with coordinates (r',θ',ϕ'). Suppose that the axis of $\mathscr{C}'$, the line $\theta'=0$, lies in the direction $\theta=\theta_0$, $\phi=\phi_0$ in $\mathscr{C}$, and also that ϕ_0 is the anticlockwise angle from the great circle $\phi=\phi_0$ to the great circle $\phi'=0$ (these two circles cross at $\theta'=0$, which is the axis of $\mathscr{C}'$). The three angles θ_0, ϕ_0 and ϕ_0' uniquely define the rotation from $\mathscr{C}$

to $\mathscr{C}'$. It can be shown that the coordinates of $\mathscr{C}$ and $\mathscr{C}'$ are related by

$$r' = r, \tag{A 4}$$

$$\cos\theta' = \sin\theta\cos(\phi-\phi_0)\sin\theta_0 + \cos\theta\cos\theta_0, \tag{A 5}$$

$$\tan(\phi'+\phi_0') = \frac{\sin\theta\sin(\phi-\phi_0)}{\sin\theta\cos(\phi-\phi_0)\cos\theta_0 - \cos\theta\sin\theta_0}. \tag{A 6}$$

Effect of rotations on the spherical harmonic functions

We note that

$$\begin{aligned}\langle Y_{mn}(\theta,\phi)Y_{m'n'}(\theta',\phi')\rangle &= -\frac{1}{s_n^2}\langle(\nabla^2 Y_{mn}(\theta,\phi))Y_{m'n'}(\theta',\phi')\rangle \\ &= -\frac{1}{s_n^2}\langle Y_{mn}(\theta,\phi)\nabla^2(Y_{m'n'}(\theta',\phi'))\rangle \\ &= \frac{s_{n'}^2}{s_n^2}\langle Y_{mn}(\theta,\phi)Y_{m'n'}(\theta',\phi')\rangle,\end{aligned} \tag{A 7}$$

where $\langle\cdot\rangle$ denotes the integral over the surface of the sphere $r=1$, and the second equality was achieved by integrating by parts twice (note that, since the surface of the sphere is closed, there are no boundary terms arising from the integrations by parts). Therefore $\langle Y_{mn}(\theta,\phi)Y_{m'n'}(\theta',\phi')\rangle$ equals zero unless $n=n'$, and we define

$$\gamma_{mm'n}(\phi_0,\theta_0,\phi_0') = \langle Y_{mn}(\theta,\phi)Y_{m'n}(\theta',\phi')\rangle. \tag{A 8}$$

Since $\hat{\boldsymbol{r}}$, and hence $\mathbb{P}_{mn}$, are invariant under rotations of the coordinate system, we have $\mathbb{P}_{mn}(\theta',\phi') = Y_{mn}(\theta',\phi')\hat{\boldsymbol{r}}$, from which it immediately follows that

$$\begin{aligned}\langle\mathbb{P}_{mn}(\theta,\phi)\cdot\mathbb{P}_{m'n'}(\theta',\phi')\rangle &= \langle Y_{mn}(\theta,\phi)Y_{m'n'}(\theta',\phi')\rangle \\ &= \gamma_{mm'n}(\phi_0,\theta_0,\phi_0')\delta_{nn'},\end{aligned} \tag{A 9}$$

$$\langle\mathbb{P}_{mn}(\theta,\phi)\cdot\mathbb{B}_{m'n'}(\theta',\phi')\rangle = 0, \tag{A 10}$$

$$\langle\mathbb{P}_{mn}(\theta,\phi)\cdot\mathbb{C}_{m'n'}(\theta',\phi')\rangle = 0. \tag{A 11}$$

We can also calculate

$$\begin{aligned}\langle\mathbb{B}_{mn}(\theta,\phi)\cdot\mathbb{B}_{m'n'}(\theta',\phi')\rangle &= \left\langle\frac{1}{s_n s_{n'}}\boldsymbol{\nabla}Y_{mn}(\theta,\phi)\cdot\boldsymbol{\nabla}Y_{m'n'}(\theta',\phi')\right\rangle \\ &= -\left\langle\frac{1}{s_n s_{n'}}Y_{mn}(\theta,\phi)\nabla^2 Y_{m'n'}(\theta',\phi')\right\rangle \\ &= \frac{s_{n'}}{s_n}\langle Y_{mn}(\theta,\phi)Y_{m'n'}(\theta',\phi')\rangle \\ &= \gamma_{mm'n}(\phi_0,\theta_0,\phi_0')\delta_{nn'},\end{aligned} \tag{A 12}$$

$$\begin{aligned}\langle\mathbb{B}_{mn}(\theta,\phi)\cdot\mathbb{C}_{m'n'}(\theta',\phi')\rangle &= \left\langle\frac{1}{s_n s_{n'}}\boldsymbol{\nabla}(Y_{mn}(\theta,\phi))\cdot\boldsymbol{\nabla}\times(Y_{m'n'}(\theta',\phi')\boldsymbol{r})\right\rangle \\ &= -\left\langle\frac{1}{s_n s_{n'}}Y_{mn}(\theta,\phi)\boldsymbol{\nabla}\cdot\boldsymbol{\nabla}\times(Y_{m'n'}(\theta',\phi')\boldsymbol{r})\right\rangle \\ &= 0\end{aligned} \tag{A 13}$$

and

$$\langle\mathbb{C}_{mn}(\theta,\phi)\cdot\mathbb{C}_{m'n'}(\theta',\phi')\rangle$$

$$
\begin{aligned}
&= \left\langle \frac{1}{s_n s_{n'}} \boldsymbol{\nabla} \times (Y_{mn}(\theta,\phi)\boldsymbol{r}) \cdot \boldsymbol{\nabla} \times (Y_{m'n'}(\theta',\phi')\boldsymbol{r}) \right\rangle \\
&= \sum_{i_5=1}^{3}\sum_{i_4=1}^{3}\sum_{i_3=1}^{3}\sum_{i_2=1}^{3}\sum_{i_1=1}^{3} \left\langle \frac{1}{s_n s_{n'}} \left(\epsilon_{i_1 i_2 i_3} \frac{\partial}{\partial x_{i_2}} (Y_{mn}(\theta,\phi) r_{i_3}) \right.\right. \\
&\quad \left.\left. \times\ \epsilon_{i_1 i_4 i_5} \frac{\partial}{\partial x_{i_4}} (Y_{m'n'}(\theta',\phi') r_{i_5}) \right) \right\rangle \\
&= \sum_{i_3=1}^{3}\sum_{i_2=1}^{3} \left\langle \frac{1}{s_n s_{n'}} \left(\frac{\partial}{\partial x_{i_2}} (Y_{mn}(\theta,\phi) r_{i_3}) \frac{\partial}{\partial x_{i_2}} (Y_{m'n'}(\theta',\phi') r_{i_3}) \right.\right. \\
&\quad \left.\left. - \frac{\partial}{\partial x_{i_2}} (Y_{mn}(\theta,\phi) r_{i_3}) \frac{\partial}{\partial x_{i_3}} (Y_{m'n'}(\theta',\phi') r_{i_2}) \right) \right\rangle \\
&= \left\langle \frac{1}{s_n s_{n'}} [-Y_{mn}(\theta,\phi)\boldsymbol{r} \cdot \nabla^2 (Y_{m'n'}(\theta',\phi')\boldsymbol{r}) \right. \\
&\quad \left. + Y_{mn}(\theta,\phi)(\boldsymbol{r}\cdot\boldsymbol{\nabla})(\boldsymbol{\nabla} \cdot (Y_{m'n'}(\theta',\phi')\boldsymbol{r}))] \right\rangle \\
&= \left\langle \frac{1}{s_n s_{n'}} [-Y_{mn}(\theta,\phi)\boldsymbol{r} \cdot (-s_{n'}^2 Y_{m'n'}(\theta',\phi')\boldsymbol{r} + 2\boldsymbol{\nabla} Y_{m'n'}(\theta',\phi')) \right. \\
&\quad \left. + Y_{mn}(\theta,\phi)(\boldsymbol{r}\cdot\boldsymbol{\nabla})(3Y_{m'n'}(\theta',\phi') + \boldsymbol{r}\cdot\boldsymbol{\nabla} Y_{m'n'}(\theta',\phi'))] \right\rangle \\
&= \left\langle \frac{s_{n'}}{s_n} Y_{mn}(\theta,\phi) Y_{m'n'}(\theta',\phi') \right\rangle = \gamma_{mm'n}(\phi_0,\theta_0,\phi_0')\delta_{nn'}, \qquad \text{(A 14)}
\end{aligned}
$$

where x_i, $i = 1, 2, 3$, denote Cartesian coordinates, $\epsilon_{i_1 i_2 i_3}$ is the alternating tensor, and its standard properties as well as the relationships $\boldsymbol{r}\cdot\boldsymbol{\nabla} Y_{mn}(\theta,\phi) = \boldsymbol{r}\cdot\boldsymbol{\nabla} Y_{m'n'}(\theta',\phi') = 0$ were used to simplify the expressions.

The above equations show that, in a rotated coordinate system, each vector spherical harmonic can be expressed as a linear combination of the vector spherical harmonics of the same family (i.e. $\mathbb{P}$, $\mathbb{B}$ or $\mathbb{C}$) and with the same value of the index n.

Rotations of the eigenfunctions

Thus the eigenfunctions written with respect to the rotated coordinates $\mathscr{C}'$ can be written with respect to $\mathscr{C}$ as

$$
\begin{aligned}
\boldsymbol{u}_{lmn}^{(1q)}(r',\theta',\phi') &= \sum_{m',n'} \langle \boldsymbol{u}_{lmn}^{(1q)}(r',\theta',\phi') \cdot \mathbb{P}_{m'n'-1}(r,\theta,\phi)\rangle \mathbb{P}_{m'n'-1}(r,\theta,\phi) \\
&\quad + \sum_{m',n'} \langle \boldsymbol{u}_{lmn}^{(1q)}(r',\theta',\phi') \cdot \mathbb{B}_{m'n'-1}(r,\theta,\phi)\rangle \mathbb{B}_{m'n'-1}(r,\theta,\phi) \\
&\quad + \sum_{m',n'} \langle \boldsymbol{u}_{lmn}^{(1q)}(r',\theta',\phi') \cdot \mathbb{C}_{m'n'-1}(r,\theta,\phi)\rangle \mathbb{C}_{m'n'-1}(r,\theta,\phi) \\
&= \left(\frac{j_{n-1}(a_{ln} r)}{r j_{n-1}(a_{ln})} - r^{n-2} \right) \sum_{m'=-(n-1)}^{n-1} \gamma_{m'mn-1}(\phi_0,\theta_0,\phi_0') \mathbb{P}_{m'n-1}(r,\theta,\phi) \\
&\quad + \left(\frac{a_{ln} r j_{n-2}(a_{ln} r) - (n-1) j_{n-1}(a_{ln} r)}{s_{n-1} r j_{n-1}(a_{ln})} - \frac{n}{s_{n-1}} r^{n-2} \right)
\end{aligned}
$$

$$\times \sum_{m'=-(n-1)}^{n-1} \gamma_{m'mn-1}(\phi_0,\theta_0,\phi_0')\mathbb{B}_{m'n-1}(r,\theta,\phi)$$

$$= \sum_{m'=-(n-1)}^{n-1} \gamma_{m'mn-1}(\phi_0,\theta_0,\phi_0')\boldsymbol{u}^{(1q)}_{lm'n}(r,\theta,\phi), \tag{A 15}$$

$$p^{(1q)}_{lmn}(r',\theta',\phi') = \sum_{m',n'} \langle p^{(1q)}_{lmn}(r',\theta',\phi')Y_{m'n'-1}(r,\theta,\phi)\rangle Y_{m'n'-1}(r,\theta,\phi)$$

$$= \sum_{m'=-(n-1)}^{n-1} \gamma_{m'mn-1}(\phi_0,\theta_0,\phi_0')p^{(1q)}_{lm'n}(r,\theta,\phi), \tag{A 16}$$

$$\boldsymbol{u}^{(2q)}_{lmn}(r',\theta',\phi') = \sum_{m'=-n}^{n} \gamma_{m'mn}(\phi_0,\theta_0,\phi_0')\boldsymbol{u}^{(2q)}_{lm'n}(r,\theta,\phi), \tag{A 17}$$

$$p^{(2q)}_{lmn}(r',\theta',\phi') = 0, \tag{A 18}$$

which leads to

$$\mathscr{V}^{(kq)}_{lmn}(r',\theta',\phi') = \sum_{m'=-\tilde{n}}^{\tilde{n}} \gamma_{m'm\tilde{n}}(\phi_0,\theta_0,\phi_0')\mathscr{V}^{(kq)}_{lm'n}(r,\theta,\phi), \tag{A 19}$$

where $\tilde{n} = n + k - 2$, and for $k = 1, 2$.

Expressing all the eigenfunctions in terms of rotations of one eigenfunction

We investigate whether a given eigenfunction $\mathscr{V}^{(kq)}_{lmn}(r,\theta,\phi)$ can be expressed in terms of a linear superposition of rotations of $\mathscr{V}^{(kq)}_{lm_0n}$, for some value m_0. We search for suitable weighting functions $W^{(k)}_{mm_0n}(\phi_0,\theta_0,\phi_0')$ that satisfy the equation

$$\mathscr{V}^{(kq)}_{lmn}(r,\theta,\phi) = \int_0^{2\pi}\int_0^{\pi}\int_0^{2\pi} W^{(k)}_{mm_0n}(\phi_0,\theta_0,\phi_0')\mathscr{V}^{(kq)}_{lm_0n}(r',\theta',\phi')\,\mathrm{d}\phi_0\,\mathrm{d}\theta_0\,\mathrm{d}\phi_0'$$

$$= \sum_{m'=-\tilde{n}}^{\tilde{n}} \left(\int_0^{2\pi}\int_0^{\pi}\int_0^{2\pi} W^{(k)}_{mm_0n}(\phi_0,\theta_0,\phi_0')\gamma_{m'm_0\tilde{n}}(\phi_0,\theta_0,\phi_0')\,\mathrm{d}\phi_0\,\mathrm{d}\theta_0\,\mathrm{d}\phi_0' \right)$$

$$\times \mathscr{V}^{(kq)}_{lm'n}(r,\theta,\phi), \tag{A 20}$$

for $W^{(k)}_{mm_0n}$. Given m, m_0 and n, this is equivalent to finding a function $W^{(k)}_{mm_0n}$ such that

$$\int_0^{2\pi}\int_0^{\pi}\int_0^{2\pi} W^{(k)}_{mm_0n}(\phi_0,\theta_0,\phi_0')\gamma_{m'm_0\tilde{n}}(\phi_0,\theta_0,\phi_0')\,\mathrm{d}\phi_0\,\mathrm{d}\theta_0\,\mathrm{d}\phi_0' = \delta_{mm'} \tag{A 21}$$

for all values of m'. To simplify this expression, we recall the definition of $\gamma_{m'm_0\tilde{n}}$, (A 8), expand the spherical harmonics (A 1), and use the relationships between the two sets of coordinates (A 4)–(A 6) to show that

$$\begin{aligned}\gamma_{m'm_0\tilde{n}}(\phi_0,\theta_0,\phi_0') &= \int_0^{2\pi}\int_0^{\pi} Y_{m'\tilde{n}}(\theta,\phi)Y_{m_0\tilde{n}}(\theta',\phi')\sin\theta\,\mathrm{d}\theta\,\mathrm{d}\phi\\ &= c_{m'\tilde{n}}c_{m_0\tilde{n}}\,\mathrm{e}^{\mathrm{i}m'\phi_0-\mathrm{i}m_0\phi_0'}\int_0^{2\pi}\int_0^{\pi}(\sin\theta)^{m'}P_{\tilde{n}}^{(m')}(\cos\theta)\mathrm{e}^{\mathrm{i}m'\tilde{\phi}}\\ &\quad\times(\sin\theta\cos\tilde{\phi}\cos\theta_0-\cos\theta\sin\theta_0+\mathrm{i}\sin\theta\sin\tilde{\phi})^{m_0}\\ &\quad\times P_{\tilde{n}}^{(m_0)}(\sin\theta\cos\tilde{\phi}\sin\theta_0+\cos\theta\cos\theta_0)\sin\theta\,\mathrm{d}\theta\,\mathrm{d}\tilde{\phi},\end{aligned}\tag{A 22}$$

where $c_{m\tilde{n}}=(-1)^m\sqrt{(2\tilde{n}+1)(\tilde{n}-m)!/(4\pi(\tilde{n}+m)!)}$, $P_{\tilde{n}}^{(m)}$ denotes the mth derivative of $P_{\tilde{n}}$ and $\tilde{\phi}=\phi-\phi_0$.

The integral does not depend on ϕ_0 or ϕ_0', and thus, for fixed θ_0, $\gamma_{m'm_0\tilde{n}}$ is proportional to $\mathrm{e}^{\mathrm{i}m'\phi_0-im_0\phi_0'}$. In order to satisfy (A 21) for all values of m', we must therefore have

$$W_{mm_0n}^{(k)}(\phi_0,\theta_0,\phi_0')=\mathrm{e}^{-\mathrm{i}m\phi_0+\mathrm{i}m_0\phi_0'}f_{mm_0n}^{(k)}(\theta_0),\tag{A 23}$$

for some function f_{mm_0n}. With this choice

$$\begin{aligned}&\int_0^{\pi}\int_0^{2\pi}\int_0^{\pi}W_{mm_0n}^{(k)}(\phi_0,\theta_0,\phi_0')\gamma_{m'm_0\tilde{n}}(\phi_0,\theta_0,\phi_0')\,\mathrm{d}\phi_0\,\mathrm{d}\theta_0\,\mathrm{d}\phi_0'\\ &\quad=\delta_{mm'}\Bigg(4\pi^2c_{mn}c_{m_0\tilde{n}}\int_0^{\pi}\int_0^{2\pi}\int_0^{\pi}f_{mm_0n}^{(k)}(\theta_0)(\sin\theta)^mP_{\tilde{n}}^{(m)}(\cos\theta)\mathrm{e}^{\mathrm{i}m\tilde{\phi}}\\ &\qquad\times(\sin\theta\cos\tilde{\phi}\cos\theta_0-\cos\theta\sin\theta_0+\mathrm{i}\sin\theta\sin\tilde{\phi})^{m_0}\\ &\qquad\times P_{\tilde{n}}^{(m_0)}(\sin\theta\cos\tilde{\phi}\sin\theta_0+\cos\theta\cos\theta_0)\sin\theta\,\mathrm{d}\theta\,\mathrm{d}\tilde{\phi}\,\mathrm{d}\theta_0\Bigg).\end{aligned}\tag{A 24}$$

The quantity multiplying $\delta_{mm'}$ on the right-hand side is a constant that depends on the choice of $f_{mm_0n}^{(k)}$. We have a considerable amount of freedom to do this. One way is to set $f_{mm_0n}^{(k)}(\theta_0)=C_k\delta(\theta_0-\theta_{00})$, where $0\leqslant\theta_{00}\leqslant\pi$ is a fixed polar angle, $\delta(\cdot)$ is the Dirac delta function and C_k is a normalization constant, chosen so that the quantity multiplying $\delta_{mm'}$ on the right-hand side of (A 24) equals 1. In the case $\theta_{00}=0$ and $\theta_{00}=\pi$, it is not possible to create all the eigenfunctions (which is to be expected), but it should be possible in most other cases. This shows that, for given values of k, l and m_0, every eigenfunction $\mathscr{V}_{lmn}^{(kq)}$ can be written as a superposition of those rotations of the eigenfunction $\mathscr{V}_{lm_0n}^{(kq)}$ for which the axis lies on the line of latitude $\theta=\theta_{00}$ (although note that, for $k=1$, the pressure needs rescaling to convert between different values of q). For example, we can express the eigenfunctions $\mathscr{V}_{lmn}^{(kq)}$ for all values of m and q as a superposition of the eigenfunctions $\mathscr{V}_{l0n}^{(kq)}$ with axis on $\theta=\pi/2$.

This argument shows that the eigenfunctions $\mathscr{V}_{lmn}^{(kq)}$ are rotations of one another for different values of m and q. It is, however, interesting that the two sums $\sum_m A_m\mathscr{V}_{lmn}^{(1q)}$ and $\sum_{m'}A_{m'}'\mathscr{V}_{lm'n}^{(2q)}$ cannot be related by a rotation for any choice of the constants A_m and $A_{m'}'$ (not all zero), even though they share the same eigenvalue.

REFERENCES

ARFKEN, G. B. & WEBER, H. J. 2001 *Mathematical Methods for Physicists*, 5th edn. IAP Harcourt Academic.

BISHOP, P. N. 2000 Structural macromolecules and supramolecular organisation of the vitreous gel. *Prog. Retinal Eye Res.* **19** (3), 323–344.

BUCHSBAUM, G., STERNKLAR, M., LITT, M., GRUNWALD, J. E. & RIVA, C. E. 1984 Dynamics of an oscillating viscoelastic sphere: a model of the vitreous humor of the eye. *Biorheology* **21**, 285–296.

DALTON, P. D., CHIRILA, T. V., HONG, Y. & JEFFERSON, A. 1995 Oscillatory shear experiments as criteria for potential vitreous substitutes. *Polym. Gels Networks* **3** (4), 429–444.

DAVID, T., SMYE, S., DABBS, T. & JAMES, T. 1998 A model for the fluid motion of vitreous humour of the human eye during saccadic movement. *Phys. Med. Biol.* **43**, 1385–1399.

DYSON, R., FITT, A. J., JENSEN, O. E., MOTTRAM, N., MIROSHNYCHENKO, D., NAIRE, S., OCONE, R., SIGGERS, J. H. & SMITHBECKER, A. 2004 Post re-attachment retinal re-detachment. In *Proceedings of the Fourth Medical Study Group*. University of Strathclyde, Glasgow.

LEE, B., LITT, M. & BUCHSBAUM, G. 1992 Rheology of the vitreous body. Part I. Viscoelasticity of human vitreous. *Biorheology* **29**, 521–533.

LEE, B., LITT, M. & BUCHSBAUM, G. 1994 Rheology of the vitreous body. Part 2. Viscoelasticity of bovine and porcine vitreous. *Biorheology* **31** (4), 327–338,.

LEONE, G., CONSUMI, M., AGGRAVI, M., DONATI, A., LAMPONI, S. & MAGNANI, A. 2010 PVA/STMP based hydrogels as potential substitutes of human vitreous. *J. Mater. Sci.: Mater. Med.* **21**, 2491–2500.

NICKERSON, C. S., PARK, J., KORNFIELD, J. A. & KARAGEOZIAN, H. 2008 Rheological properties of the vitreous and the role of hyaluronic acid. *J. Biomech.* **41** (9), 1840–1846.

QUARTAPELLE, L. & VERRI, M. 1995 On the spectral solution of the three-dimensional Navier–Stokes equations in spherical and cylindrical regions. *Comput. Phys. Commun.* **90**, 1–43.

REPETTO, R., SIGGERS, J. H. & STOCCHINO, A. 2008 Steady streaming within a periodically rotating sphere. *J. Fluid Mech.* **608** 71–80.

REPETTO, R., SIGGERS, J. H. & STOCCHINO, A. 2010 Mathematical model of flow in the vitreous humor induced by saccadic eye rotations: effect of geometry. *Biomech. Model. Mechanobiol.* **9** (1), 65–76.

REPETTO, R., STOCCHINO, A. & CAFFERATA, C. 2005 Experimental investigation of vitreous humour motion within a human eye model. *Phys. Med. Biol.* **50**, 4729–4743.

SCOTT, J. D. 2002 Future perspectives in primary retinal detachment repair. *Eye* **16** (4), 349–352.

SOMAN, N. & BANERJEE, R. 2003 Artificial vitreous replacements. *Biomed. Mater. Engng* **13** (1), 59–74.

SWINDLE, K., HAMILTON, P. & RAVI, N. 2008 In situ formation of hydrogels as vitreous substitutes: viscoelastic comparison to porcine vitreous. *J. Biomed. Mater. Res.* A **87A** (3), 656–665.

SWINDLE, K. E. & RAVI, N. 2007 Recent advances in polymeric vitreous substitutes. *Exp. Rev. Ophthalmol.* **2** (2), 255–265.

SWINDLE-REILLY, K. E., SHAH, M., HAMILTON, P. D., ESKIN, T. A., KAUSHAL, S. & RAVI, N. 2009 Rabbit study of an in situ forming hydrogel vitreous substitute. *Invest. Ophthalmol. Vis. Sci.* **50** (10), 4840–4846.

TANNER, R. I. 2000 *Engineering Rheology*, 2nd edn. Oxford University Press.

WALTON, K. A., MEYER, C. H., HARKRIDER, C. J., COX, T. A. & TOTH, C. A. 2002 Age-related changes in vitreous mobility as measured by video B scan ultrasound. *Exp. Eye Res.* **74** (2), 173–180.

ZIMMERMAN, R. L. 1980 In vivo measurements of the viscoelasticity of the human vitreous humor. *Biophys. J.* **29**, 539–544.